New Journal of Physics
The open access journal at the forefront of physics

Deutsche Physikalische Gesellschaft DPG IOP Institute of Physics

PAPER • OPEN ACCESS

Eigenvalue measurement of topologically protected edge states in split-step quantum walks

To cite this article: Thomas Nitsche *et al* 2019 *New J. Phys.* **21** 043031

New Journal of Physics
The open access journal at the forefront of physics

Deutsche Physikalische Gesellschaft DPG
IOP Institute of Physics

Published in partnership with: Deutsche Physikalische Gesellschaft and the Institute of Physics

OPEN ACCESS

RECEIVED
16 November 2018

REVISED
1 February 2019

ACCEPTED FOR PUBLICATION
25 March 2019

PUBLISHED
15 April 2019

PAPER

Eigenvalue measurement of topologically protected edge states in split-step quantum walks

Thomas Nitsche[1], **Tobias Geib**[2], **Christoph Stahl**[2], **Lennart Lorz**[1], **Christopher Cedzich**[2,3], **Sonja Barkhofen**[1], **Reinhard F Werner**[2] and **Christine Silberhorn**[1]

[1] Applied Physics, University of Paderborn, Warburger Straße 100, D-33098 Paderborn, Germany
[2] Institut für Theoretische Physik, Leibniz Universität Hannover, Appelstr. 2, D-30167 Hannover, Germany
[3] Institut für Theoretische Physik, Universität zu Köln, Zülpicher Straße 77, D-50937 Köln, Germany

E-mail: tnitsche@mail.upb.de

Keywords: quantum walks, topological phenomena, symmetry protected edge states, split-step, bulk-boundary correspondence, decoupling

Abstract

We study topological phenomena of quantum walks by implementing a novel protocol that extends the range of accessible properties to the eigenvalues of the walk operator. To this end, we experimentally realise for the first time a split-step quantum walk with decoupling, which allows for investigating the effect of a bulk-boundary while realising only a single bulk configuration. The experimental platform is implemented with the well-established time-multiplexing architecture based on fibre-loops and coherent input states. The symmetry protected edge states are approximated with high similarities and we read-out the phase relative to a reference for all modes. In this way we observe eigenvalues which are distinguished by the presence or absence of sign flips between steps. Furthermore, the results show that investigating a bulk-boundary with a single bulk is experimentally feasible when decoupling the walk beforehand.

1. Introduction

Phenomena such as the quantum Hall effect [1] and topological insulators [2, 3] aroused vivid interest in the study of the topological properties of physical systems. While these effects have been originally observed in semiconductor systems, experimental studies have been conducted on systems such as ultra cold atoms [4–7], photonic model systems [8–12], solid-state systems [13, 14], superconducting circuits [15], mechanical oscillators [16] and microwave networks [17–19]. In photonic systems, topological phenomena can be accessed by implementing a split-step quantum walk on a 1D optical lattice [20–22].

The concept of quantum random walks extends the model of classical random walks by taking the effects of interference into consideration. It has been established for two different scenarios, namely the continuous-time and the discrete-time version. The continuous-time quantum walk is defined by a Hamiltonian including nearest neighbour hopping, while discrete-time quantum walks (DTQW) describe the discrete time evolution of a walker with an internal degree of freedom on a lattice. An extensive account on the relation of discrete- and continuous-time quantum walks from view-point of mathematical physics can be found in [23, 24]. The interference effects allow quantum walks to spread quadratically faster than their classical counterparts, which recently raised much interest in quantum walks as a computational resource [25–27]. Moreover, quantum walks exhibit a rich variety of single-particle quantum effects such as Landau–Zener tunnelling [28], the Klein paradox [29] or the formation of molecules [30]. Recently, a uniform framework for coupling external gauge fields to quantum walks has been established [31] which contains the one-dimensional electric walks studied in [32] as a special case. Possible experimental implementations include nuclear magnetic resonance [33, 34], trapped ions [35, 36] and atoms [37, 38]. Considering photonic systems, translating the walker in the spatial degree of freedom might seem most straight-forward [39–46], however, implementations utilising time as the external

degree of freedom outperform spatiallly multiplexed systems in terms of resource efficiency and stability [47–53]. Other possible degrees of freedom include spectral distributions or orbital angular momentum [54, 55].

So far, the experimental investigation of topological phenomena has been focused on the demonstration of edge states, i.e. eigenstates of the systems, while eigenvalues of the walk operator have not been measured. Employing a phase-reference method, in which we selectively interfere components of walker's wavefunction assigned to a certain step, position and polarisation with a reference of well-controlled phase, we are for the first time able to measure not only the intensities related to the eigenfunctions, but also the signs related to the eigenvalues of the walk operator. This work also constitutes the first experimental implementation of a split-step quantum walk with decoupling as proposed in [56, 57], which allows for investigating the effect of a bulk-boundary while realising only a single bulk configuration. Such a scheme thus not only requires a smaller set of different coin angles that have to be implemented, but also reduces the size of the space occupied by the walk, freeing positions which can now be used for routing of the phase-reference. We implement this split-step quantum walk system exhibiting a bulk-boundary with decoupling by making use of a photonic platform [47] that allows for the read-out of the spatial and the coin degree of freedom as well as for dynamic coin operations [58].

In our work, we build on the comprehensive topological classification framework for infinite 1D lattices laid out in [57]. It predicts the emergence of symmetry protected edge states at the boundary of bulks with different symmetry indices. These symmetry protected eigenfunctions of the walks operator belong to the eigenvalues ± 1, which lie in the band gap of the system. Whereas the minimal number of these edge states is an invariant quantity, their associated eigenvalue ($+1$ or -1) may change under local perturbations and hence the eigenvalues of edge states for half-chain quantum walks are not robust against local perturbation. We will investigate this behaviour for an experimental realisation of the split-step quantum walk.

The article is structured as follows: we start with the definition of a (DTQW) in section 2, followed by an introduction to the topological classification of 1D quantum walks in section 2.1, then present split-step quantum walks in section 2.3, the relation between chiral symmetry and topological phases in section 2.4, the concept of decoupling in section 2.5, the concrete settings in section 2.6 as well as the expected eigenfunctions and eigenvalues in section 2.7. We then turn to the experimental concepts, namely the physical implementation in section 3.1, the eigenstate distillation in section 3.2 and the phase-reference method in section 3.3. The results concerning the evolution of the wavefunction and the validation of the eigenvalues are presented in sections 4.1 resp. 4.2. Finally, the conclusion is drawn in section 5.

2. Theoretical background

Discrete time quantum walks describe the discrete time evolution of a *walker* with an internal degree of freedom on the lattice. We here focus on the spatially one-dimensional case where at each site of the lattice the internal degree of freedom is described by the finite-dimensional *coin space* $\mathcal{C}^d$. Consequently, the overall Hilbert space is $\mathcal{H} = \ell^2(\mathcal{Z}) \otimes \mathcal{C}^d$. A quantum walk W is a unitary operator on $\mathcal{H}$ which obeys a locality condition and determines the discrete time evolution of a state $|\psi(t)\rangle \in \mathcal{H}$ by

$$|\psi(t+1)\rangle = W|\psi(t)\rangle. \tag{1}$$

The locality of W means that in a single time step an initially localised state can jump only by a finite number of lattice sites. We remark that the classification in [57] allows for more general notions of locality, but bounding the jump length is sufficient for this paper.

A constructive way to define quantum walks, which is handy for experimental realisations and automatically fulfils the locality condition, is the concept of *coined quantum walks*. For these the walk operator W is build from a finite sequence of *conditional shifts* and *coin operations*: Denoting by $|x\rangle \in \ell^2(\mathcal{Z})$ and $|i\rangle \in \mathcal{C}^d$ basis vectors of the position and coin space, respectively, conditional shifts and coin operations act on basis vectors of $\mathcal{H}$ by

$$C|x, i\rangle = \sum_j C_{ij}(x)|x, j\rangle \quad \text{and} \quad S_j|x, i\rangle = |x + \delta_{ij}, i\rangle. \tag{2}$$

The coin operation C acts locally in each cell, whereas the conditional shift S_j ($S_j^\dagger$) shifts the j-component of the coin space to the right (left) while leaving the other internal degrees of freedom unchanged. Both operators are unitaries, such that W is also guaranteed to be unitary. In this definition, the maximal jump-length of the walk is bounded from above, by the number of shift operations in the sequence constituting W.

In our experimental realisation the coin-space is two-dimensional and the basis vectors are implemented by horizontal and vertical polarisation, which we denote by $|H\rangle$ and $|V\rangle$, respectively. The quantum walks which are modelled in the experiment are of the form

$$W = S_{\mathrm{H}} S_{\mathrm{V}}^{\dagger} C_1 S_{\mathrm{H}} S_{\mathrm{V}}^{\dagger} C_2, \tag{3}$$

with possibly different coins C_1 and C_2, which will be specified later in sections 2.3 and 2.6.

Note, that in general one might define a one-dimensional quantum walk abstractly as a unitary on a doubly infinite direct sum of possibly different finite dimensional Hilbert spaces $\mathcal{H}_x$: $\mathcal{H} = \bigoplus_{x\in\mathbb{Z}} \mathcal{H}_x$. The locality condition is then stated as

$$\langle \psi_x | W \psi_y \rangle = 0 \quad \text{for all } \psi_x \in \mathcal{H}_x,\ \psi_y \in \mathcal{H}_y \text{ with } |x-y| > L, \tag{4}$$

for some $L < \infty$. The general theory for the topological classification of symmetric quantum walks, which will be sketched in the next section, demands an even less strict definition of locality. There the matrix elements $\langle \psi_x | W \psi_y \rangle$ are only assumed to decay sufficiently fast with $|x-y|$.

2.1. Topological classification of one-dimensional quantum walks

With this setting in mind, let us sketch the topological classification of symmetric quantum walks given in [57]. Below we apply the results provided here to discuss the topological classification of the experimentally implemented model.

A crucial assumption in [57] is that the quantum walks under consideration are 'symmetric', i.e. there is a group of discrete, involutive symmetries which either commute or commute up to taking the adjoint with the walks.

Concretely, we distinguish the following unitary and anti-unitary symmetries:

chiral symmetry: $\gamma W \gamma^{\dagger} = W^{\dagger}$, with γ unitary,

particle–hole symmetry: $\eta W \eta^{\dagger} = W$, with η anti-unitary,

time-reversal symmetry: $\tau W \tau^{\dagger} = W^{\dagger}$, with τ anti-unitary.

The groups generated by these symmetries either contain only one or all three, since any two of them multiply to the third, and they constitute the symmetry types of the tenfold way [57, 59, 60]. By the above relations, the ± 1-eigenspaces of symmetric quantum walks are invariant under these symmetries. Consequently, we assume the bulk systems under consideration to be gapped at these symmetry-invariant points, similar to the Hamiltonian setting[4].

The topological classification of symmetric quantum walks is concerned with two questions: (1) which symmetric quantum walks may be continuously connected without breaking either the symmetries, the gap condition or locality, and (2) which walks may be transformed into each other by perturbing one of them locally. In contrast to the continuous time setting, these questions are fundamentally different: In the unitary discrete-time setting there are local perturbations that cannot be contracted, which is due to the extra symmetry invariant point in the spectrum at -1 [57]. The classification in [57] answers these questions by assigning the three *symmetry indices* si_-, si_+, and $\overrightarrow{\mathrm{si}}$ to each symmetric quantum walk. Here, $\mathrm{si}_\pm$ characterise the ± 1-eigenspaces and their values cannot be changed by continuous symmetric deformations. On the other hand, the *right symmetry index* $\overrightarrow{\mathrm{si}}$ is a bulk invariant that characterises the evolution asymptotically far on the right half-chain. It is also invariant under continuous deformations, but in contrast to $\mathrm{si}_\pm$ also cannot be changed by locally perturbing the system.

2.2. Emergence of symmetry protected edge states

An important physical consequence of this topological classification of symmetric quantum walks is the *bulk-boundary correspondence*: whenever two bulks are joined spatially, the absolute value of the difference of their right symmetry indices $\overrightarrow{\mathrm{si}}$ is a lower bound for the number of symmetry protected edge states which appear near the interface region. These edge states have eigenvalues ± 1 and are therefore stable against continuous deformations that respect the symmetries. Since these symmetry protected edge states are the only eigenfunctions observed in the concrete examples below, we occasionally refer to them simply as eigenfunctions.

In order to provide experimental evidence for the emergence of symmetry protected edge states one typically measures the position distribution of a time evolved initial state. This is, however, not sufficient to reveal their topological nature since the emergence of localised states near a local perturbation is a typical phenomenon [30, 62]. Instead, in this publication we demonstrate a direct eigenvalue measurement to give evidence that the observed edge states are indeed symmetry protected.

[4] In the general theory of [56, 57, 61] quantum walks satisfy the relations of a symmetry type and are gapped at the symmetry-invariant points are called *admissible*.

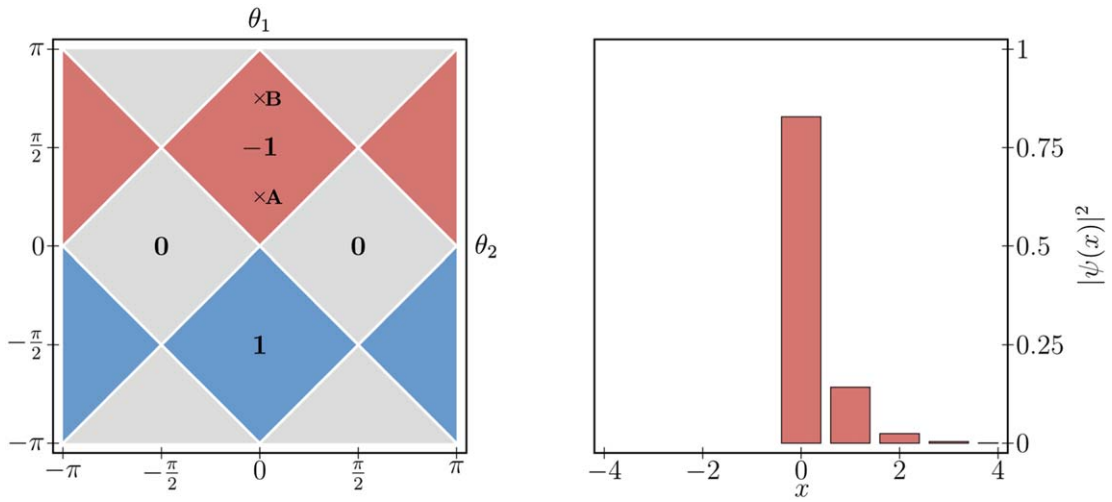

Figure 1. Left: parameter plane for the split-step walk (5) with regions of constant index. The values are determined by the winding number of (9). The crosses mark the parameters for our two settings (**A**/**B**). Right: Intensity distribution $|\psi(x)|^2$ of the corresponding eigenfunctions (21), restricted to the even sublattice. The distribution is the same for both settings.

The appearance of symmetry protected edge states does not depend on how the crossover between two symmetric systems is designed. A particularly simple scenario in which such edge states emerge is given by decoupling a walk operator W locally to a walk $W' = W_L \oplus W_R$ which has zero transition amplitudes between the right and left half chain of the cut. Such decouplings exist for every walk and every symmetry type and can even be chosen to be a continuous perturbation [57]. Depending only on the right half-chain, the right symmetry index $\overrightarrow{\mathrm{si}}(W) = \mathrm{si}(W_R)$ of W may then be calculated as the combined symmetry indices si_- and si_+ of the right half-chain walk, i.e. $\overrightarrow{\mathrm{si}}(W) = \mathrm{si}_+(W_R) + \mathrm{si}_-(W_R)$.

However, whether the symmetry protected edge states correspond to the eigenvalue $+1$ or -1 depends on the choice of crossover, since in contrast to their sum $\overrightarrow{\mathrm{si}}(W)$, the indices $\overrightarrow{\mathrm{si}}_\pm(W) = \mathrm{si}_\pm(W_R)$ themselves are not stable under local perturbations. Exactly this dependence of $\overrightarrow{\mathrm{si}}_\pm(W)$ on the crossover will be analysed and experimentally validated in the present publication by choosing different decouplings.

2.3. Split-step quantum walks

Emblematic for coined quantum walks is the so-called *split-step quantum walk* [20]. It is defined on $\mathcal{H} = \ell_2(\mathcal{Z}) \otimes \mathcal{C}^2$ as the coined quantum walk

$$W(\theta_1, \theta_2) = S_\downarrow C(\theta_1) S_\uparrow C(\theta_2), \tag{5}$$

where $S_\uparrow = S_H$ and $S_\downarrow = S_V^\dagger$ (compare (2)) shift the internal basis state $|H\rangle \in \mathcal{C}^2$ to the right and $|V\rangle$ to the left, respectively. The coin operation

$$C(\theta) = \mathrm{e}^{-\mathrm{i}\theta\sigma_x} = \begin{pmatrix} \cos(\theta) & -\mathrm{i}\sin(\theta) \\ -\mathrm{i}\sin(\theta) & \cos(\theta) \end{pmatrix} \tag{6}$$

rotates the internal degree of freedom by an angle θ around the σ_x-axis. Note that the split-step walk is typically defined with rotations around the σ_y-axis. Since these two implementations are unitarily equivalent and in the experiment described below we implement the σ_x-rotation, we take (5) with coin (6) as the definition of the split-step walk. The walk (5) is of symmetry type BDI, i.e. it is chiral, time-reversal and particle–hole symmetric with each symmetry squaring to the identity. Moreover, it exhibits a rich structure of topological phases, and therefore has become the working example in many publications concerning topological effects in quantum walks [9, 20, 21, 61, 63]. Figure 1 shows the different topological phases of the split-step quantum walk. The interactive web tool in [64] allows the user to explore how the eigenfunctions and the symmetry indices of the split-step walk change with modifications of the parameters θ_1 and θ_2 as well as for different decouplings.

The quantum walk we implement in the experiment described below is a model related to the split-step walk. It is defined by

$$W = SC(\theta_1) SC(\theta_2), \tag{7}$$

where $S = S_\mathrm{H} S_\mathrm{V}^\dagger$ denotes the bidirectional conditional shift. Since this walk protocol contains two such shift operations, a walker which is initially localised on even (odd) positions, never leaves the even (odd) sub-lattice. Thus, on each of these sublattices the walk (7) implements effectively a split-step walk with doubled jump length. Since our initial states will always be localised at $x = 0$, we restrict considerations to the even sub-lattice from

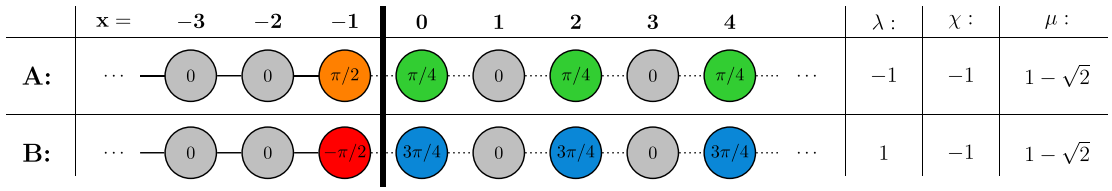

Figure 2. Schematic picture of the coin angle set-up for the walk (7) in our two settings. The coin angles at $x = -1$ decouple the walk between $x = -1$ and $x = 0$. λ denotes the eigenvalue, χ the chirality and μ the decay coefficient of the edge state, respectively.

now on. Rescaling this even sub-lattice by $x \mapsto x/2$ the effective walk we implement in the experiment is the split-step walk defined in (5).

2.4. Chiral symmetry and topological phases

Being of symmetry type BDI the effective split-step walk has chiral symmetry, i.e. there exists a unitary γ with $\gamma^2 = +\mathbb{1}$ such that $\gamma W \gamma^\dagger = W^\dagger$. This symmetry operator is given by

$$\gamma = \bigoplus_{x\in\mathbb{Z}} \gamma_0, \quad \text{with} \quad \gamma_0 = \begin{pmatrix} -\sin(\theta_2) & -\mathrm{i}\cos(\theta_2) \\ \mathrm{i}\cos(\theta_2) & \sin(\theta_2) \end{pmatrix}, \tag{8}$$

where the θ_2-dependence of γ is due to the choice of the local bases: conjugating with $C(\theta_2/2)$ gives $C(\theta_2/2)\gamma_0 C(-\theta_2/2) = \sigma_y$.

For translation invariant chiral symmetric walks with $\gamma^2 = +\mathbb{1}$, the symmetry index $\vec{\mathrm{si}}$ is given by the winding number of a certain matrix block of the walk operator in momentum space. Since the derivation of the formula would exceed the discussion here, we only sketch the relevant relations. The complete derivation can be found in [61, proposition 3.9]. Being translation invariant, the split-step quantum walk gets mapped to a continuous matrix valued function $\widehat{W}(k)$ of the quasi momentum k by the discrete Fourier transformation $\mathcal{F}\colon \ell^2(\mathcal{Z}) \otimes \mathcal{C}^2 \to \mathcal{L}^2([-\pi, \pi)) \otimes \mathcal{C}^2$. If we now switch to a chiral eigenbasis (e.g. by conjugating with $U = C(\theta_2/2 + \pi/4)$), the symmetry index is given by the winding of the upper right matrix element

$$(U\widehat{W}(k)U^\dagger)_{12} = -\mathrm{i}(\sin(\theta_1)\cos(\theta_2) + \cos(\theta_1)\sin(\theta_2)\cos(k) - \mathrm{i}\cos(\theta_1)\sin(k)), \tag{9}$$

as a complex valued function of $k \in [-\pi, \pi)$. The corresponding values of the index are shown in the parameter plane in figure 1. Compare also [64] for a visualisation of the winding function (9). Note, that there the order of θ_1 and θ_2 is interchanged and the coin rotations are defined as $R(\theta) = \exp(\mathrm{i}\theta\sigma_y)$, resulting in a clockwise $\pi/2$ rotation of the parameter plane in figure 1.

2.5. Decoupling

To construct a decoupling for the split-step walk we make use of its special form. Replacing in (5) the local coin $C(\theta_1)$ at $x = 0$ by a reflective coin, i.e. a coin whose diagonal elements are zero, decouples the resulting walk between $x = 0$ and $x = -1$. To reproduce this decoupled split-step setting as an effective sublattice walk of the experimentally accessible walk, we need to replace the coin $C(\theta_1)$ at $x = -1$ in (7).

The decoupling coins within the parameter regions are the rotations by angles $\theta = \pm\pi/2$, for which (6) indeed has only zeros on the diagonal. Whenever a walk in a non-trivial phase, i.e. with non-vanishing $\vec{\mathrm{si}}$ is decoupled, exponentially localised eigenstates are predicted at the interface by bulk-boundary correspondence. As remarked above, however, it depends on the specific decoupling whether these eigenfunctions correspond to the eigenvalue $+1$ or -1. These two possibilities can be distinguished by an additional (walk specific) invariant, namely $\vec{\mathrm{si}}_-(W) = \mathrm{si}_-(W_R)$ of the decoupled walk $W' = W_L \oplus W_R$.

2.6. Settings for the experimental implementation

We consider two settings with different values for the coin. In both settings the effective walks have non-trivial symmetry index and are decoupled between $x = -1$ and $x = 0$. The aim is to determine the eigenvalues of the eigenfunctions emerging to the right at the boundary, i.e. on $\mathcal{H}_R = \bigoplus_{x\geqslant 0}\mathcal{H}_x$. The two settings for (7) are the following (see figure 2):

Setting **A:**

$$\theta_2 = \pi/4 \qquad \text{and} \qquad \theta_1(x) = \begin{cases} \pi/2 & x = -1 \\ 0 & \text{else} \end{cases} \tag{10}$$

Setting **B:**

$$\theta_2 = 3\pi/4 \qquad \text{and} \qquad \theta_1(x) = \begin{cases} -\pi/2 & x = -1 \\ 0 & \text{else} \end{cases}. \tag{11}$$

In both cases θ_1 is chosen to decouple the walk on the even sub-lattice. We do not need to specify the left half chain here, since we are only interested in edge states of the decoupled walk located to the right. Hence, only the coin configuration for $x > 0$ determines the phase of the effective walk, and we infer from the phase diagram in figure 1 that in both settings the corresponding symmetry index is $\vec{\mathrm{si}}(W_{\mathbf{A/B}}) = -1$, which predicts the emergence of edge states.

2.7. Eigenfunctions and eigenvalues

To compute the eigenfunctions of W in both settings, we first note that W and γ commute on the ± 1-eigenspaces of W. Therefore, we can jointly diagonalize W and γ on these eigenspaces. The (un-normalised) eigenvectors φ_0^χ of γ_0 in (8) are of the form

$$\varphi_0^\chi = \begin{pmatrix} \mathrm{i}\cos(\theta_2) \\ -(\sin(\theta_2) + \chi) \end{pmatrix}, \tag{12}$$

where $\chi \in \{+1, -1\}$ denotes the chirality, i.e. the eigenvalue of γ. Since edge-states of decoupled translation invariant systems have to decay exponentially in the bulk [61] and we are only interested in eigenfunctions of the walk W located to the right, we choose the following ansatz:

$$\phi_\lambda^\chi(x) = \begin{cases} 0 & x < 0 \\ a \cdot \varphi_0^\chi & x = 0, \\ \mu^x \varphi_0^\chi & x > 0 \end{cases} \quad \text{fulfilling the eigenvalue equation} \quad W\phi_\lambda^\chi = \lambda\phi_\lambda^\chi. \tag{13}$$

Here, the free parameter a takes care of the boundary condition which is determined by the choice of the decoupling coin, and μ denotes the exponential decay rate away from the boundary. Note that ϕ_0^χ is normalizable if $|\mu| < 1$. To solve for μ, we evaluate the eigenvalue equation in the bulk, i.e. without taking the boundary into account. This leads to

$$0 = \lambda\cos(\theta_2)\mu - \chi\sin(\theta_2) - 1, \tag{14}$$

$$0 = \chi\cos(\theta_2)\mu - \lambda\sin(\theta_2) - \chi\lambda, \tag{15}$$

which are solved by

$$\mu(\lambda, \chi) = \frac{1 + \chi\sin(\theta_2)}{\lambda\cos(\theta_2)}. \tag{16}$$

In both settings **A** and **B** with $\theta_2 = \pi/4$ and $\theta_2 = 3\pi/4$, respectively, we have

$$|\mu(-1, 1)| = |\mu(1, 1)| = |1 + \sqrt{2}| > 1, \tag{17}$$

$$|\mu(-1, -1)| = |\mu(1, -1)| = |1 - \sqrt{2}| < 1. \tag{18}$$

Therefore, by the condition $|\mu| < 1$ in our setting the eigenfunction located to the right of the bulk must have chirality $\chi = -1$.

In order to determine a we have to take into account the boundary condition. Choosing the solutions of the eigenvalue equation with $\chi = -1$ leads to the following equations for a:

$$0 = a\cos(\theta_2)(\lambda + \sin(\theta_1)), \tag{19}$$

$$0 = (a - 1)(1 - \sin(\theta_2))\lambda. \tag{20}$$

Note that the first equation is actually independent of a whenever $a \neq 0$. Hence, the first equation rules out one of the two possibilities in (18). We get $\lambda = -1$ for $\theta_1 = \pi/2$ (setting **A**) and $\lambda = 1$ for $\theta_1 = -\pi/2$ (setting **B**). In both settings, however, we must have $a = 1$ for the second equation to be satisfied.

Inserting a, χ and λ into (12), (13) and (16), we get the following eigenfunctions located to the right

$$\phi_R(x) = \begin{cases} 0 & x < 0 \\ c(1 - \sqrt{2})^x \begin{pmatrix} \mathrm{i}\cos(\theta_2) \\ 1 - \sin(\theta_2) \end{pmatrix} & x \geqslant 0, \end{cases} \tag{21}$$

with the normalisation factor $c = ((1 + \sqrt{2})(1 - \sin(\theta_2))^{-\frac{1}{2}}$ and $\theta_2 = \pi/4$ for setting **A** and $\theta_2 = 3\pi/4$ for setting **B**, respectively. Note, that in both settings $\mu(\lambda, \chi)$ takes the same value $(1 - \sqrt{2})$.

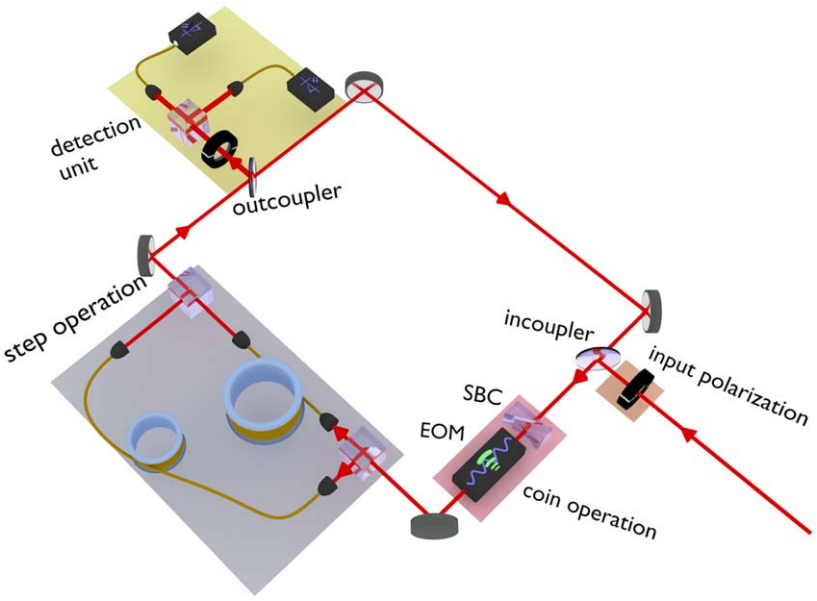

Figure 3. Schematic of our setup: the light is coupled in and out of the setup with probabilistic in- and outcouplers. The coin operation is carried out with a static Solei–Babinet compensator (SBC) and a dynamic electro-optic modulator (EOM). The step operation is carried out by splitting the light into two fibres of different length. The detection unit allows for polarisation-resolved read-out.

3. Experimental implementation

3.1. Time-multiplexing setup

The realisation of the two described settings and the direct measurement of the eigenvalues require a stable, flexible experimental platform, as a phase-stable evolution incorporating a dynamic coin operation has to be ensured over a sufficiently large number of steps. Our system of choice relies on a well-established time-multiplexed architecture utilising fibre loops for DTQW [47, 48, 50]. The dynamic coin operation implemented with a fast-switching electro-optic modulator (EOM) makes it suitable for a wide range of experiments, including the investigation of topological phenomena [22, 58].

Previous photonic implementations allowed for accessing topological invariants associated with probability distributions or amplitudes within a certain step of the walk [9, 22, 65–69]. However, topological properties can also manifest themselves in the emergence of eigenstates with associated eigenvalues that are revealed by the phase relation between the walker's wavefunctions for two consecutive steps. So far, this phase relation has not been investigated experimentally. By interfering the walker with a reference of fixed phase, we are now able to probe this feature as well.

Our implementation relies on a photonic walker implemented by an attenuated coherent laser pulse with its polarisation representing the internal (coin) degree of freedom. In this way, our system makes use of the equivalence of coherent light and a single quantum particle when propagating in a linear optical network [70].

Figure 3 shows the physical implementation of the quantum walk setup: Our time-multiplexing architecture relies on translating the external (position) degree of freedom of the walker into the time domain by splitting the pulses up spatially, routing them through fibres of different length and subsequently merging the two paths again. This translation in time corresponds to the shift operation according to (2). The ratio of this probabilistic splitting taking place at polarising beam splitters (PBS) is determined by the polarisation state of the walker. This internal degree of freedom is acted upon by coin operations (see (6)) implemented with static (Soleil–Babinet compensator (SBC)) and dynamic (EOM based on Pockels cell, EOM) polarisation optics. The remarkable characteristic of the EOM is that its switching speed allows for addressing individual positions within the walk. This dynamic coin enables us to implement an alternating coin needed for the split-step scheme (see (10) and (11)) as well as the reflecting and transmitting coin operations indispensable in directing the reference pulse along a certain path (see section 3.3). Note that implementing a protocol according to (7) means that an actual step in the quantum walk requires two roundtrips through the setup. The polarisation degree of freedom can also be accessed in the read-out process, since our detection unit comprising another PBS and 2 avalanche photo-diodes is polarisation-resolving.

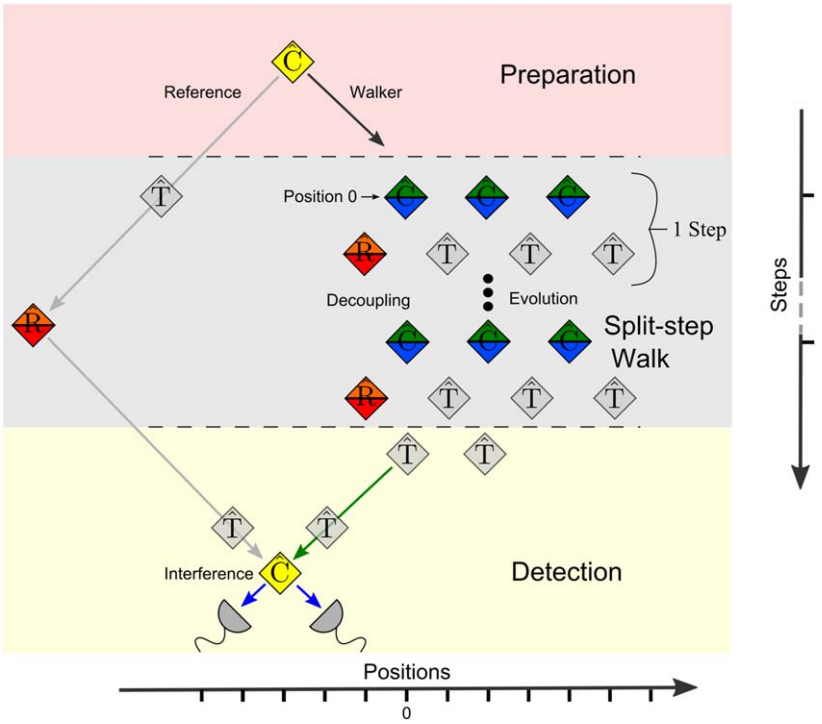

Figure 4. Schematic of our implementation of a split-step quantum walk followed by a phase readout via the interference method. Squares with $\hat{T}$ denote a transmission operation, while $\hat{R}$ refers to reflection and $\hat{C}$ to mixing coins, for which the exact form can be different depending on setting and position.

3.2. Eigenstate distillation

Since the exponentially localised eigenstate cannot be excited directly with an initial state just occupying one position, we need a method to prepare an approximate eigenstate of the system. In order to do so, we make use of the spreading behaviour of the split-step quantum walk. In systems for which the translational invariance is only broken at the edge, the eigenstates are exponentially localised [61]. If we choose an initial state near a boundary and let the system evolve for some time, the components of the state which have no overlap with the localised state will propagate away from the boundary, while the content which overlaps will stay. Consequently, we concentrate our study onto the three positions near the boundary, which is justified due to the exponential decay of the state (see equation (21)). By renormalizing the remaining state, we prepare an approximate eigenfunction. For quantifying how closely we have approached the theoretically expected distribution, we use the similarity which is obtained by summing up the square roots of the products of the theoretical and experimental probabilities for the relevant positions within the step that is examined. It can possibly assume values between 0 (no overlap of intensities) and 1 (perfect overlap of intensities)

$$d = \left| \sum_x \sqrt{P_{\mathrm{H},x}^{(\mathrm{theo})} \cdot P_{\mathrm{H},x}^{(\mathrm{exp})}} + \sum_x \sqrt{P_{\mathrm{V},x}^{(\mathrm{theo})} \cdot P_{\mathrm{V},x}^{(\mathrm{exp})}} \right|. \tag{22}$$

3.3. Phase-reference method

Figure 4 illustrates how the dynamic coin operation can be harnessed to implement a split-step quantum walk followed by a phase readout via the interference method: by applying a mixing coin at the initial position (marked $\hat{C}$) the walker is split into a vertical component travelling through the shorter fibre, i.e. being translated to the left in the schematic and a horizontal component running through the longer fibre, which corresponds to a translation to the right. The part going to the left constitutes the reference. In order to prevent it from mixing with the split-step walk taking place on the right as well as from losing intensity to positions that are not on the desired path, the EOM switches to identity (marked $\hat{T}$ for transmission in figure 4) on the positions where the reference is found. For the phase read-out the reference needs to interfere with the light having undergone the walk, so the travelling direction is inverted by switching a reflection (marked $\hat{R}$ in figure 4) in the middle of the propagation.

The light translated to the right in the initial splitting constitutes the input state of the split-step quantum walk with decoupling. The decoupling is realised by a reflection operation implemented on the decoupling

position. The split-step walk (see (10) and (11)) incorporates a mixing coin (indicated by $\hat{C}$ in figure 4) on even positions and the identity coin, corresponding to a transmission operation, on uneven positions.

The scheme shown in figure 4, (a) brings the reference to interfere with the vertical light ending up at position 0 of the split-step walk. At the position where the light from the walk and reference interfere a mixing coin has to be applied. The ratio of the intensities at the two detection positions (marked by detectors) then allows obtaining information on the phase relation. All polarisations, positions and steps can be accessed analogously, as long as the proper routing of the reference and the pulse under investigation can be ensured. The basic principle remains the same in all runs, but the actual positions of the switchings differ. For this purpose, a flexible dynamic coin operation is indispensable.

We access two regimes with topologically different eigenvalues by applying a coin of either $\hat{C}_{\mathrm{EV}-1} = \mathrm{e}^{-\mathrm{i}\sigma_x \cdot \frac{\pi}{4}}$ for an eigenvalue of -1 (setting **A**, (10)) or $\hat{C}_{\mathrm{EV}+1} = \mathrm{e}^{-\mathrm{i}\sigma_x \cdot \frac{3}{4}\pi}$ for an eigenvalue of $+1$ (setting **B**, (11)) and $\hat{T} = \mathrm{e}^{-\mathrm{i}\sigma_x \cdot 0\pi} = \mathbb{1}$ for the transmission as well as $\hat{R} = \mathrm{e}^{-\mathrm{i}\sigma_x \cdot \frac{\pm\pi}{2}}$ for the reflection. All of these coins can be implemented with a combination of static SBC and dynamic EOM operations.

The interference of a certain component of the walker with the reference together with the application of a mixing coin (in this case the balanced Hadamard coin $\hat{C}_{\mathrm{Had}}$) results in the following expression for the wavefunction at the position where the interference takes place (labelled 'Interference' in figure 4):

$$|\Phi\rangle = \hat{C}_{\mathrm{Had}} \begin{pmatrix} \mathrm{e}^{\mathrm{i}\alpha_{\mathrm{w}}}\sqrt{I_{\mathrm{w}}} \\ \mathrm{e}^{\mathrm{i}\alpha_{\mathrm{r}}}\sqrt{I_{\mathrm{r}}} \end{pmatrix} = \frac{1}{\sqrt{2}} \begin{pmatrix} 1 & 1 \\ 1 & -1 \end{pmatrix} \begin{pmatrix} \mathrm{e}^{\mathrm{i}\alpha_{\mathrm{w}}}\sqrt{I_{\mathrm{w}}} \\ \mathrm{e}^{\mathrm{i}\alpha_{\mathrm{r}}}\sqrt{I_{\mathrm{r}}} \end{pmatrix}. \tag{23}$$

Here α_{w} and α_{r} denote the phase of the walker resp. of the reference. $\sqrt{I_{\mathrm{w}}}$ and $\sqrt{I_{\mathrm{r}}}$ are the square roots of the walker's and the reference's intensities. The detected intensities I_{H} and I_{V} for the horizontal and the vertical detector are then given by the following expression:

$$\begin{aligned} I_{\mathrm{H}} &= \frac{1}{2}(I_{\mathrm{w}} + I_{\mathrm{r}} - 2\sqrt{I_{\mathrm{w}}} \cdot \sqrt{I_{\mathrm{r}}}\sin(\alpha_{\mathrm{r}} - \alpha_{\mathrm{w}}))) \\ I_{\mathrm{V}} &= \frac{1}{2}(I_{\mathrm{w}} + I_{\mathrm{r}} + 2\sqrt{I_{\mathrm{w}}} \cdot \sqrt{I_{\mathrm{r}}}\sin(\alpha_{\mathrm{r}} - \alpha_{\mathrm{w}}))). \end{aligned} \tag{24}$$

Thus we can deduce the phase difference between the reference and a certain component of the walker from the measured intensities at the read-out positions (marked by a detector symbol in figure 4):

$$M = \sin(\alpha_{\mathrm{r}} - \alpha_{\mathrm{w}}) = \frac{I_{\mathrm{V}} - I_{\mathrm{H}}}{2\sqrt{I_{\mathrm{w}}} \cdot \sqrt{I_{\mathrm{r}}}}. \tag{25}$$

Note that the M-parameter given by this formula is $\sin(\alpha_{\mathrm{r}} - \alpha_{\mathrm{w}})$, which is not an injective function. However, it still provides a clear distinction between cases in which we expect an eigenvalue of 1 and cases with an eigenvalue of -1.

Distinguishing these eigenvalues requires monitoring how the M-parameter changes from step to step. For an eigenvalue of -1 (setting **A**), the walker's phase α_{w} is expected to change by π, while for an eigenvalue of 1 (setting **B**) it is either 0 or integer multiples of 2π. Since the phase of the reference α_{r} can be assumed to be constant for all numbers of steps, monitoring the step-wise evolution of the M-parameter for the two settings should clearly reveal the different eigenvalues. In the experiment, the eigenvalues will be manifested in the relative intensities of horizontal and vertical light at the read-out positions. Accessing the eigenvalues requires the read-out of both polarisations for the three inner positions. Furthermore, the state of the walker over 3 steps (6, 7 and 8) is monitored. Since each measurement just yields information for a certain position, polarisation and step, obtaining the full information makes 18 individual measurement runs necessary. Observing the differences between settings **A** and **B** doubles the number of measurements required, so that eventually 36 data sets have to be taken.

4. Results

As outlined previously, the experiment aims at accessing the evolution of eigenvalues over three consecutive steps. As we are limited by losses to numbers of physical roundtrips around 22, the actual state of the walker will constitute an approximation of the ideal eigenstate. We quantify the quality of the approximation by calculating the similarity between the experimental intensity and the ideal eigenstate according to (22). Furthermore, the phase-reference method indicates the eigenvalue of the system under investigation.

4.1. Evolution of the wavefunction

As a certain proportion of the intensity is outcoupled in each roundtrip, we are able to monitor its temporal evolution. Figure 5 shows the evolution for six steps of a split-step quantum walk and the subsequent read-out of

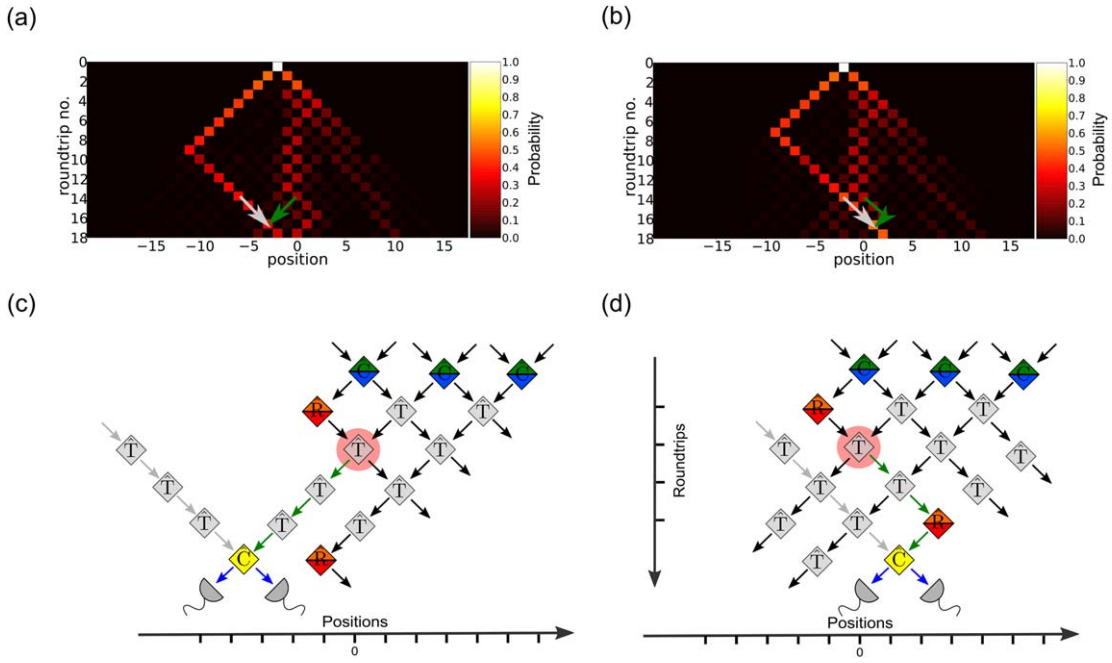

Figure 5. Plot of the intensity (polarisation is traced out) evolution for six steps (12 roundtrips) of a split-step quantum walk and the subsequent read-out of the vertical (a) resp. the horizontal component (b) at position 0. Subfigures (c) and (d) illustrate the corresponding read-out schemes: either the vertical (c) or the horizontal (d) component (marked by green arrows) from the read-out position (marked by red dot) is brought to interference with the reference (grey arrows). Transmission and reflection operations are conducted such that light coming from other positions or polarisations (black arrows) does not end up in the time bins reserved for analysing the interference between reference and read-out component (marked by detector symbols). Note that the exact position of the interference is chosen such that it allows for separating one component from the others and for having the read-out in the same step for both polarisations.

the vertical (a) resp. the horizontal component (b) at position 0. Note that in this nomenclature 0 corresponds to the innermost position of the eigenstate and not to the position at which the light pulse starts (see figure 4).

The plots illustrate how the reference is steered with transmission and reflection operations on the left-hand side (marked by a grey arrow) and is then brought to interference with either the vertical or the horizontal component (green arrow) of the walker evolving on the right-hand side. From the distribution of intensity between the two detection bins the M-parameter can be inferred according to equation (25). During the split-step quantum walk up to roundtrip 13, the intensity on the right-hand side either concentrates near position 0 or runs out towards the right. In order to quantify the overlap of this intensity near position 0 with the theoretically expected eigenstate, we calculate the similarity according to (22) for the three innermost positions (see figure 6).

While in step 6 the similarity between experiment and the ideal eigenfunction exhibits values of 0.891 ± 0.019 (eigenvalue -1) resp. 0.929 ± 0.029 (eigenvalue $+1$), in step 8 these values attain 0.979 ± 0.024 (eigenvalue -1) resp. 0.984 ± 0.029 (eigenvalue $+1$), getting almost as close to the ideal value of 1 as the numerically predicted state. The numerical simulation accounts for the limited number of steps but no other experimental imperfections, it thus quantifies the effects of the finite system size in correspondence to the deviation from the ideal similarity of 1. The difference between the numerically and the experimentally determined similarity is accordingly due to further experimental imperfections such as slightly inhomogeneous losses or imperfect EOM switchings. The high values of the similarity give evidence for the successful outcome of the distillation process. Note that the difference between numerical and experimental values is slightly larger for the scenario with eigenvalue -1, presumably due to the fact that here the EOM needs to switch a larger coin angle and thus the applied voltage needs to be higher. Consequently, experimental imperfections, e.g. due to resonances of the Pockels cell used in the EOM, which are hard to quantify in an error model and subject to ongoing investigation, are increased for the eigenvalue -1 case.

4.2. Eigenvalues

Having quantified the overlap of the measured intensities with the ideal eigenstates, the focus now shifts on measuring the eigenvalues of the walk operator. We therefore monitor the evolution of the M-parameter (see (25)) from step 6 to step 8 for a rotation angle $\theta_{\mathbf{A}} = 1/4\pi$, for which theory predicts an eigenvalue $\lambda = -1$, and $\theta_{\mathbf{B}} = 3/4\pi$, associated in theory with an eigenvalue of $+1$. This analysis is done for both horizontal and vertical polarisation, which require separate read-out procedures as explained above.

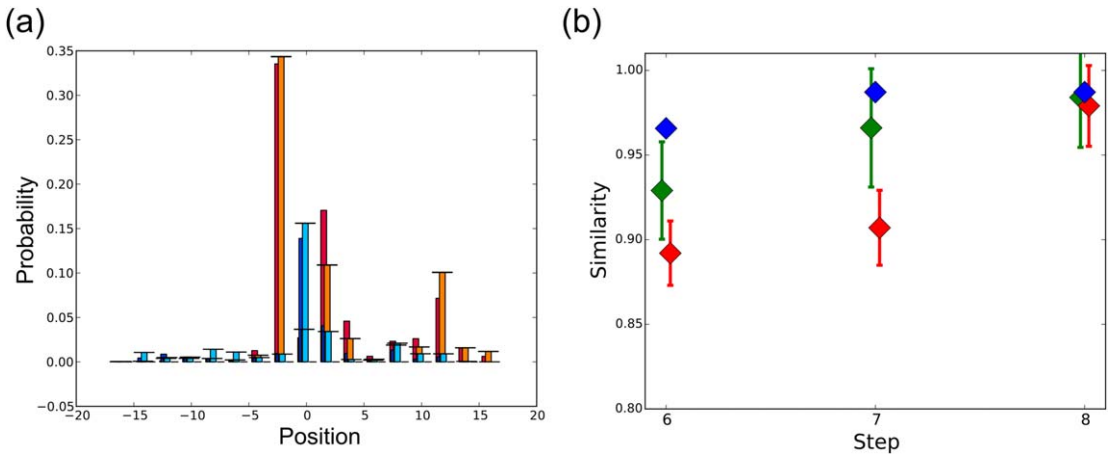

Figure 6. (a) Probability distribution in step 8 (roundtrip 17) of the split-step quantum walk. Orange (red) bar charts represent the experimental (numerical) probabilities for horizontal light, while light blue (dark blue) bar charts corresponds to experimental (numerical) data for vertical light. The large horizontal bar at positon −2 stands for the phase reference, while the components around position 10 are those not overlaping with the eigenstate. (b) The similarity according to (22) between the ideal eigenstate and the numerically determined state for finite step numbers (blue markers, the same for both eigenvalues) as well as the similarity between the ideal state and the experimentally obtained state for both the regimes with eigenvalue +1 (green markers) and eigenvalue −1 (red markers). Note that all markers correspond to integer step numbers, even though they are slightly shifted on the horizontal axis for better readability.

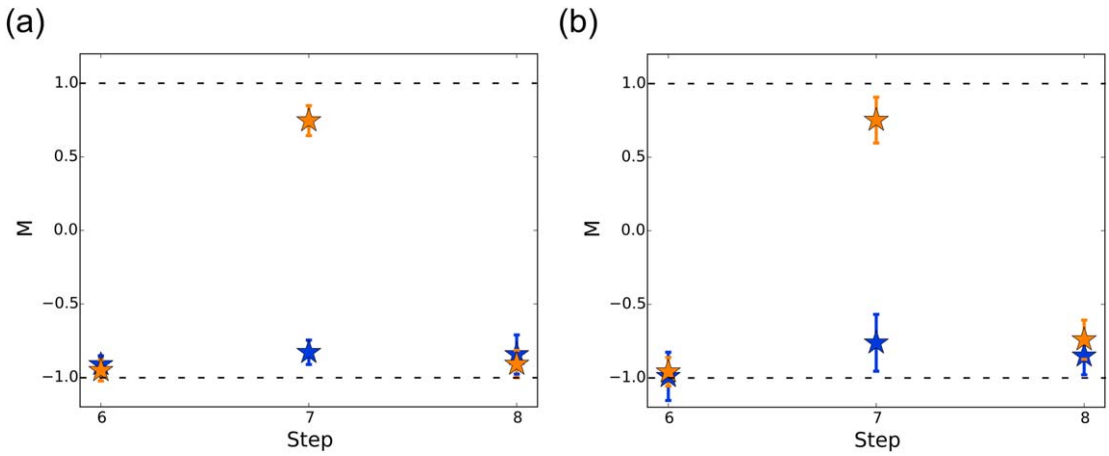

Figure 7. The evolution of the *M*-parameter (see (25)) for position 0 from step 6 to 8 for both horizontally (a) and vertically (b) polarised light. The orange markers correspond to setting **A** with Eigenvalue −1 and the blue markers to setting **B** with Eigenvalue 1. The error bars are obtained in a Monte-Carlo-Simulation accounting for the effects of an error of the coupling efficiency of 2% and an error of the coin angle of 2° (discussed in section 4.3).

Figure 7 shows the evolution of the M-parameter (see (25)) for horizontal (a) and vertical (b) polarisation at position 0. Setting **A** with Eigenvalue −1 (orange markers) and setting **B** with Eigenvalue +1 (blue markers) are clearly distinguishable for both polarisations. However, the results for vertical polarisation exhibit larger error bars as we measure a more unbalanced ratio of the intensity of the walker and the intensity of the reference. This is due to the fact that the theoretical eigenstate as well as its experimental approximation show significantly less intensity in vertical polarisation than in horizontal polarisation, while the reference remains the same in both cases.

The amplitudes of the eigenstates decrease by a factor of $(1-\sqrt{2})$ when the position is increased by one (see (21)). Accordingly, the errors get bigger when reading out position 1 (see figure 8). For horizontal polarisation (figure 8 (a)) the results still reflect the theoretically expected behaviour with larger error bars than for position 0, while for vertical polarisation a quantification of the M-parameter is no longer possible in the eighth step, as the measured intensity of the walker is not significantly above the noise floor.

4.3. Error discussion

The eigenstate validation as well as the read-out of the *M*-parameter require the measurement of intensity distributions. These distributions are subjected to inhomogeneities of the coupling efficiencies and inaccuracies

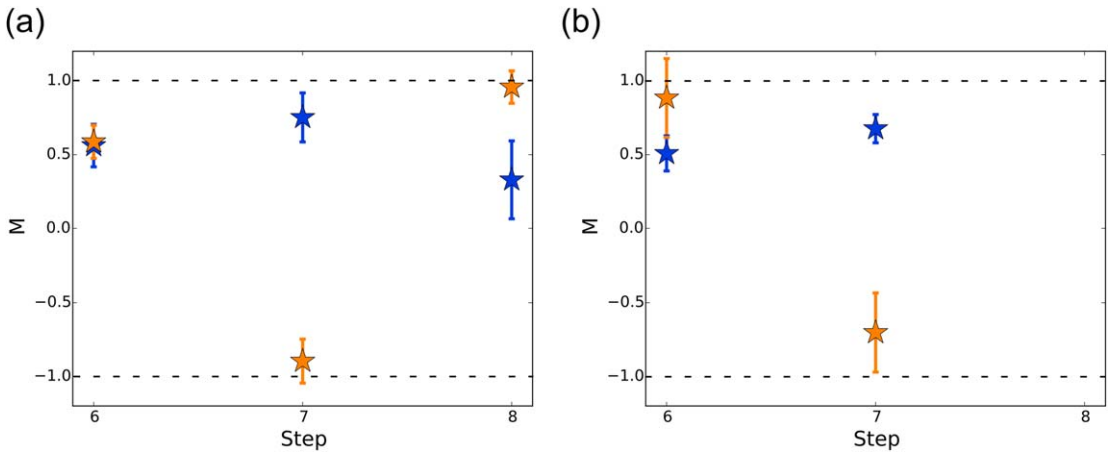

Figure 8. The evolution of the M-parameter as in figure 7, except now for position 1. Note that the amplitude scaling of the eigenstate does not allow for the read-out of the vertical component in step 8.

in the angles of the statically and dynamically implemented coins. Assuming errors of the coupling efficiencies of 2% and of the coin angle of 2°, we conduct a Monte-Carlo simulation in which we randomly generate 1000 different settings for these quantities within the assumed error range. For each of these settings we calculate the deviation of the resulting numeric intensity distribution from a reference intensity distribution. This is obtained when running the numerical simulation with the fit parameters allowing for the closest approximation of the experimental results. The error for the individual positions and polarisations is then calculated as the standard deviation of the randomly generated samples from the reference distribution. Eventually, the errors of the similarity and the M-parameter are determined via error propagation from the errors of the intensities, resulting in the error bars visible in figures 6–8.

As discussed in section 3.2, the eigenstates cannot be directly excited, but only be approximated via distillation during the evolution of the walker. The resulting deviations from the ideal eigenstates are quantified via the experimentally obtained similarities which are discussed in section 4.1.

5. Conclusion

We implemented a split-step quantum walk with decoupling over step numbers ranging from 6 to 8, requiring up to 22 roundtrips in the setup. At the end of the evolution, the states in the experiment approximate the localised eigenstates with similarities of up to 0.979 ± 0.024 resp. 0.984 ± 0.029. In addition, the phase-reference method allows for measuring eigenvalues, clearly revealing two regimes with different eigenvalues for position 0. At position 1, lower intensities make the read-out more challenging, but still allow to clearly see the sign flip. The application of the phase-reference method relies on the correct implementation of the decoupling. Our setup does not only allow for decoupling, but also serves to demonstrate that the actual decoupling coin affects the eigenvalue. In our setup the possibilities to read out the internal degree as well as to dynamically apply different coins to different positions thus allow for investigating new aspects of topological quantum walks. As the eigenvalues of approximate eigenstates could not be measured in previous experiments, our experiment significantly extends the range of accessible topological signatures.

Acknowledgements

The group at Paderborn acknowledges financial support from the Gottfried Wilhelm Leibniz-Preis (grant number SI1115/3-1) and from the European Commission with the ERC project QuPoPCoRN (no. 725366).

The group at Hannover acknowledges support from the DFG with the SFB 1227 DQmat and from the ERC grant DQSIM.

CC acknowledges support from the Excellence Initiative of the German Federal and State Governments (ZUK 81) and the DFG (project B01 of CRC 183).

ORCID iDs

Thomas Nitsche https://orcid.org/0000-0002-8353-4563

References

[1] Klitzing K v, Dorda G and Pepper M 1980 New method for high-accuracy determination of the fine-structure constant based on quantized Hall resistance *Phys. Rev. Lett.* **45** 494–7
[2] Kane C L and Mele E J 2005 Z2 topological order and the quantum spin Hall effect *Phys. Rev. Lett.* **95** 146802
[3] König M, Wiedmann S, Brüne C, Roth A, Buhmann H, Molenkamp L W, Qi X-L and Zhang S-C 2007 Quantum spin Hall insulator state in HgTe quantum wells *Science* **318** 766–70
[4] Aidelsburger M, Lohse M, Schweizer C, Atala M, Barreiro J T, Nascimbène S, Cooper N R, Bloch I and Goldman N 2015 Measuring the Chern number of Hofstadter bands with ultracold bosonic atoms *Nat. Phys.* **11** 162–6
[5] Mancini M *et al* 2015 Observation of chiral edge states with neutral fermions in synthetic Hall ribbons *Science* **349** 1510–3
[6] Stuhl B K, Lu H-I, Aycock L M, Genkina D and Spielman I B 2015 Visualizing edge states with an atomic Bose gas in the quantum Hall regime *Science* **349** 1514–8
[7] Groh T, Brakhane S, Alt W, Meschede D, Asbóth J K and Alberti A 2016 Robustness of topologically protected edge states in quantum walk experiments with neutral atoms *Phys. Rev.* A **94** 013620
[8] Hafezi M, Demler E A, Lukin M D and Taylor J M 2011 Robust optical delay lines with topological protection *Nat. Phys.* **7** 907–12
[9] Kitagawa T, Broome M A, Fedrizzi A, Rudner M S, Berg E, Kassal I, Aspuru-Guzik A, Demler E and White A G 2012 Observation of topologically protected bound states in photonic quantum walks *Nat. Commun.* **3** 882
[10] Rechtsman M C, Zeuner J M, Plotnik Y, Lumer Y, Podolsky D, Dreisow F, Nolte S, Segev M and Szameit A 2013 Photonic Floquet topological insulators *Nature* **496** 196–200
[11] Bellec M, Michel C, Zhang H, Tzortzakis S and Delplace P 2017 Non-diffracting states in one-dimensional Floquet photonic topological insulators *Europhys. Lett.* **119** 14003
[12] Mukherjee S, Chandrasekharan H K, Öhberg P, Goldman N and Thomson R R 2018 State-recycling and time-resolved imaging in topological photonic lattices *Nat. Commun.* **9** 4209
[13] Xiong J, Kushwaha S K, Liang T, Krizan J W, Hirschberger M, Wang W, Cava R J and Ong N P 2015 Evidence for the chiral anomaly in the Dirac semimetal Na3Bi *Science* **350** 413–6
[14] Gooth J *et al* 2017 Experimental signatures of the mixed axial-gravitational anomaly in the Weyl semimetal NbP *Nature* **547** 324–7
[15] Flurin E, Ramasesh V V, Hacohen-Gourgy S, Martin L S, Yao N Y and Siddiqi I 2017 Observing topological invariants using quantum walks in superconducting circuits *Phys. Rev.* X **7** 031023
[16] Süsstrunk R and Huber S D 2015 Observation of phononic helical edge states in a mechanical topological insulator *Science* **349** 47–50
[17] Wang Z, Chong Y, Joannopoulos J D and Soljačić M 2009 Observation of unidirectional backscattering-immune topological electromagnetic states *Nature* **461** 772–5
[18] Hu W, Pillay J C, Wu K, Pasek M, Shum P P and Chong Y D 2015 Measurement of a topological edge invariant in a microwave network *Phys. Rev.* X **5** 011012
[19] Poli C, Bellec M, Kuhl U, Mortessagne F and Schomerus H 2015 Selective enhancement of topologically induced interface states in a dielectric resonator chain *Nat. Commun.* **6** 6710
[20] Kitagawa T, Rudner M, Berg E and Demler E 2010 Exploring topological phases with quantum walks *Phys. Rev.* A **82** 033429
[21] Asbóth J K 2012 Symmetries, topological phases, and bound states in the one-dimensional quantum walk *Phys. Rev.* B **86** 195414
[22] Barkhofen S, Nitsche T, Elster F, Lorz L, Gábris A, Jex I and Silberhorn C 2017 Measuring topological invariants in disordered discrete-time quantum walks *Phys. Rev.* A **96** 033846
[23] Strauch F W 2006 Connecting the discrete- and continuous-time quantum walks *Phys. Rev.* A **74** 030301
[24] Childs A M 2010 On the relationship between continuous- and discrete-time quantum walk *Commun. Math. Phys.* **294** 581–603
[25] Santha M 2008 Quantum walk based search algorithms *Proc. TAMC'08* pp 31–46
[26] Magniez F, Nayak A, Roland J and Santha M 2011 Search via quantum walk *Siam. J. Comput.* **40** 142–64
[27] Lovett N B, Cooper S, Everitt M, Trevers M and Kendon V 2010 universal quantum computation using the discrete-time quantum walk *Phys. Rev.* A **81** 042330
[28] Oka T, Konno N, Arita R and Aoki H 2005 Breakdown of an electric-field driven system: a mapping to a quantum walk **94** 100602
[29] Kurzyński P 2008 Relativistic effects in quantum walks: Klein's paradox and Zitterbewegung *Phys. Lett.* A **372** 6125–9
[30] Ahlbrecht A, Alberti A, Meschede D, Scholz V B, Werner A H and Werner R F 2012 Molecular binding in interacting quantum walks *New J. Phys.* **14** 073050
[31] Cedzich C, Geib T, Werner A H and Werner R F 2019 Quantum walks in external gauge fields *J. Math. Phys.* **60** 012107
[32] Cedzich C, Rybár T, Werner A H, Alberti A, Genske M and Werner R F 2013 Propagation of quantum walks in electric fields *Phys. Rev. Lett.* **111** 160601
[33] Du J, Li H, Xu X, Shi M, Wu J, Zhou X and Han R 2003 Experimental implementation of the quantum random-walk algorithm *Phys. Rev.* A **67** 042316
[34] Ryan C A, Laforest M, Boileau J C and Laflamme R 2005 Experimental implementation of a discrete-time quantum random walk on an NMR quantum-information processor *Phys. Rev.* A **72** 062317
[35] Schmitz H, Matjeschk R, Schneider C, Glueckert J, Enderlein M, Huber T and Schaetz T 2009 Quantum walk of a trapped ion in phase space *Phys. Rev. Lett.* **103** 090504
[36] Zähringer F, Kirchmair G, Gerritsma R, Solano E, Blatt R and Roos C F 2010 Realization of a quantum walk with one and two trapped ions *Phys. Rev. Lett.* **104** 100503
[37] Karski M, Förster L, Choi J-M, Steffen A, Alt W, Meschede D and Widera A 2009 Quantum walk in position space with single optically trapped atoms *Science* **325** 174–7
[38] Genske M, Alt W, Steffen A, Werner A H, Werner R F, Meschede D and Alberti A 2013 Electric quantum walks with individual atoms *Phys. Rev. Lett.* **110** 190601
[39] Perets H, Lahini Y, Pozzi F, Sorel M, Morandotti R and Silberberg Y 2008 Realization of quantum walks with negligible decoherence in waveguide lattices *Phys. Rev. Lett.* **100** 1–4
[40] Peruzzo A *et al* 2010 Quantum walks of correlated photons *Science* **329** 1500–3
[41] Broome M A, Fedrizzi A, Lanyon B P, Kassal I, Aspuru-Guzik A and White A G 2010 Discrete single-photon quantum walks with tunable decoherence *Phys. Rev. Lett.* **104** 153602
[42] Owens J O *et al* 2011 Two-photon quantum walks in an elliptical direct-write waveguide array *New J. Phys.* **13** 075003
[43] Sansoni L, Sciarrino F, Vallone G, Mataloni P, Crespi A, Ramponi R and Osellame R 2012 Two-particle bosonic–fermionic quantum walk via integrated photonics *Phys. Rev. Lett.* **108** 010502

[44] Di Giuseppe G, Martin L, Perez-Leija A, Keil R, Dreisow F, Nolte S, Szameit A, Abouraddy A F, Christodoulides D N and Saleh B E A 2013 Einstein-podolsky-rosen spatial entanglement in ordered and anderson photonic lattices *Phys. Rev. Lett.* **110** 150503
[45] Poulios K *et al* 2014 Quantum walks of correlated photon pairs in two-dimensional waveguide arrays *Phys. Rev. Lett.* **112** 143604
[46] Xue P, Qin H, Tang B and Sanders B C 2014 Observation of quasiperiodic dynamics in a one-dimensional quantum walk of single photons in space *New J. Phys.* **16** 053009
[47] Schreiber A, Cassemiro K N, Potoček V, Gábris A, Mosley P J, Andersson E, Jex I and Silberhorn C 2010 Photons walking the line: a quantum walk with adjustable coin operations *Phys. Rev. Lett.* **104** 050502
[48] Schreiber A, Cassemiro K N, Potoček V, Gábris A, Jex I and Silberhorn C 2011 Decoherence and disorder in quantum walks: from ballistic spread to localization *Phys. Rev. Lett.* **106** 180403
[49] Regensburger A, Bersch C, Hinrichs B, Onishchukov G, Schreiber A, Silberhorn C and Peschel U 2011 Photon propagation in a discrete fiber network: an interplay of coherence and losses *Phys. Rev. Lett.* **107** 233902
[50] Schreiber A, Gábris A, Rohde P P, Laiho K, Štefaňák M, Potoček V, Hamilton C, Jex I and Silberhorn C 2012 A 2d quantum walk simulation of two-particle dynamics *Science* **336** 55–8
[51] Jeong Y-C, Di Franco C, Lim H-T, Kim M S and Kim Y-H 2013 Experimental realization of a delayed-choice quantum walk *Nat. Commun.* **4** 2471
[52] Boutari J, Feizpour A, Barz S, Di Franco C, Kim M S, Kolthammer W S and Walmsley I A 2016 Large scale quantum walks by means of optical fiber cavities *J. Opt.* **18** 094007
[53] He Y *et al* 2017 Time-bin-encoded boson sampling with a single-photon device *Phys. Rev. Lett.* **118** 190501
[54] Bouwmeester D, Marzoli I, Karman G, Schleich W and Woerdman J 1999 Optical Galton board *Phys. Rev.* A **61** 1–9
[55] Cardano F *et al* 2015 Quantum walks and wavepacket dynamics on a lattice with twisted photons *Sci. Adv.* **1** e1500087
[56] Cedzich C, Grünbaum F A, Stahl C, Velázquez L, Werner A H and Werner R F 2016 Bulk-edge correspondence of one-dimensional quantum walks *J. Phys. A: Math. Theor.* **49** 21LT01
[57] Cedzich C, Geib T, Grünbaum F A, Stahl C, Velázquez L, Werner A H and Werner R F 2018 The topological classification of one-dimensional symmetric quantum walks *Ann. Henri Poincaré* **19** 325–83
[58] Nitsche T, Elster F, Novotný J, Gábris A, Jex I, Barkhofen S and Silberhorn C 2016 Quantum walks with dynamical control: graph engineering, initial state preparation and state transfer *New J. Phys.* **18** 063017
[59] Altland A and Zirnbauer M R 1997 Nonstandard symmetry classes in mesoscopic normal-superconducting hybrid structures *Phys. Rev.* B **55** 1142–61
[60] Kitaev A, Lebedev V and Feigel'man M 2009 *Periodic table for Topological Insulators and Superconductors* (New York: AIP) pp 22–30
[61] Cedzich C, Geib T, Stahl C, Velázquez L, Werner A H and Werner R F 2018 Complete homotopy invariants for translation invariant symmetric quantum walks on a chain *Quantum* **2** 95
[62] Ashcroft N W and Mermin N D 1976 *Solid State Physics* (New York: Holt, Rinehart and Winston)
[63] Kitagawa T 2012 Topological phenomena in quantum walks: elementary introduction to the physics of topological phases *Quantum Inf. Process.* **11** 1107–48
[64] Stahl C Interactive tool at https://qig.itp.uni-hannover.de/bulkedge/sse
[65] Cardano F *et al* 2017 Detection of Zak phases and topological invariants in a chiral quantum walk of twisted photons *Nat. Commun.* **8** 15516
[66] Zhan X, Xiao L, Bian Z, Wang K, Qiu X, Sanders B C, Yi W and Xue P 2017 Detecting topological invariants in nonunitary discrete-time quantum walks *Phys. Rev. Lett.* **119** 130501
[67] Chen C *et al* 2018 Observation of topologically protected edge states in a photonic two-dimensional quantum walk *Phys. Rev. Lett.* **121** 100502
[68] Wang X, Xiao L, Qiu X, Wang K, Yi W and Xue P 2018 Detecting topological invariants and revealing topological phase transitions in discrete-time photonic quantum walks *Phys. Rev.* A **98** 013835
[69] Xu X-Y *et al* 2018 Measuring the winding number in a large-scale chiral quantum walk *Phys. Rev. Lett.* **120** 260501
[70] Paul H and Jex I 2004 *Introduction to Quantum Optics* (Cambridge: Cambridge University Press)